Circulatory bubble dynamics: From physical to biological aspects

CrossMark

Virginie Papadopoulou [a,b,*], Meng-Xing Tang [a], Costantino Balestra [b,c],
Robert J. Eckersley [d], Thodoris D. Karapantsios [e,*]

[a] Department of Bioengineering, Imperial College London, London, UK
[b] Environmental & Occupational Physiology Lab., Haute Ecole Paul Henri Spaak, Brussels, Belgium
[c] DAN Europe Research Division, Belgium
[d] Biomedical Engineering Department, Division of Imaging Sciences, King's College London, London, UK
[e] Department of Chemistry, Aristotle University of Thessaloniki, Thessaloniki, Greece

ARTICLE INFO

ABSTRACT

Bubbles can form in the body during or after decompression from pressure exposures such as those undergone by scuba divers, astronauts, caisson and tunnel workers. Bubble growth and detachment physics then becomes significant in predicting and controlling the probability of these bubbles causing mechanical problems by blocking vessels, displacing tissues, or inducing an inflammatory cascade if they persist for too long in the body before being dissolved. By contrast to decompression induced bubbles whose site of initial formation and exact composition are debated, there are other instances of bubbles in the bloodstream which are well-defined. Gas emboli unwillingly introduced during surgical procedures and ultrasound microbubbles injected for use as contrast or drug delivery agents are therefore also discussed. After presenting the different ways that bubbles can end up in the human bloodstream, the general mathematical formalism related to the physics of bubble growth and detachment from decompression is reviewed. Bubble behavior in the bloodstream is then discussed, including bubble dissolution in blood, bubble rheology and biological interactions for the different cases of bubble and blood composition considered.

© 2014 The Authors. Published by Elsevier B.V. Open access under CC BY-NC-ND license.

Contents

* Corresponding authors.
  E-mail addresses: virginie.papadopoulou07@imperial.ac.uk (V. Papadopoulou), karapant@chem.auth.gr (T.D. Karapantsios).

1. Introduction: aim and scope

The physics of bubble growth and detachment is routinely discussed with respect to engineering applications, for example to design optimal pipes for oil transport, propeller design, flotation devices etc. [1,4]. There are however also instances where bubbles form or are introduced in vivo. In these cases the bubbles can be found in the bloodstream or in tissues. Bubble growth and detachment physics then becomes significant in predicting and controlling the probability of these bubbles causing mechanical problems by blocking vessels, displacing tissues, or inducing an inflammatory cascade if they persist for too long in the body before being dissolved.

These bubbles in the bloodstream may result in ischemic problems from direct vessel occlusion, which can be fatal in the arterial side of the circulation. Bubbles in the vasculature can obstruct blood flow, activate inflammatory pathways and cause clotting [5]. The interaction of the bubbles with the components of the blood is complex. It has been shown for instance that an adhesion force causing bubbles to lodge in the vasculature is created by the interaction between the macromolecules in the blood and the bubble which pushes it towards the endothelium [6].

This review presents the mathematical formalism related to the physics of bubble growth from decompression and attempts to discuss it in the context of bubbles in the human bloodstream. The nucleation process from hyperbaric decompression has been the primary focus of a previous publication [7] and will therefore only be briefly mentioned here, concentrating instead on the growth phase. Modeling bubble growth in the circulation can help determine the probability of them blocking the circulation directly in a given region. In addition, it is important for the determination of their persistence and rheology in the circulation, also related to the inflammation cascade, by modeling the introduced microbubble flow rate in the mixed venous blood from formation sites.

Most work in the field of decompression induced bubble growth has not been done in the in vivo context of interest here (human bloodstream), but primarily in the fields of geology (volcanic eruptions, magmas, etc.) and industrial applications (multiphase dynamics, bubbly flows in pipes, etc.) [8,12]. In addition the exact composition of the bubbles that form in vivo due to hyperbaric decompression and initial site of formation of those bubbles remain somewhat open questions [7].

By contrast to decompression induced bubbles whose site of initial formation and exact composition are debated, there are other instances of bubbles in the bloodstream which are well-defined. These are gas emboli unwillingly introduced during surgical procedures and ultrasound microbubbles injected for use as contrast or drug delivery agents. We will therefore present the general bubble growth formalism and its inertially controlled growth case in particular, before classifying the analytical or for the most part numerical solutions of the key equations with respect to the different simplifications used. Blood is then discussed as a flowing liquid where bubbles grow and detach. We finish by looking into what we can learn from the behavior of bubbles in the human bloodstream, specifically bubble dissolution, rheology and biological interactions for the different cases of bubble and blood composition considered.

2. Background: how can bubbles end up in the bloodstream?

Bubbles introduced in the circulation can have iatrogenic causes: either as a side effect of vascular and heart surgery, injections and skin transplants or on purpose in the case of embolotherapy or ultrasound contrast agents where bubbles are used to respectively deliver drugs to targeted sites or image the vasculature. Furthermore endogenous bubbles can also form in the body due to mechanical heart valves or during or after decompression from pressure exposures such as those undergone by scuba divers and astronauts and are therefore an occupational hazard for caisson and tunnel workers as well. Table 1 presents a brief summary of the characteristics of these different bubbles.

2.1. Bubbles introduced in the bloodstream on purpose

Ultrasound imaging has the advantage of being a non-invasive, non-ionizing and low-cost imaging modality. It uses sound waves (typically between 1 and 15 MHz high-frequency pressure waves) to visualize organs and blood flow. However compared to other imaging modalities such as MRI or CT, the images produced are sometimes of lower quality due to excessive attenuation (absorption, scattering and reflection) and distortion from the reflectivity of tissue boundaries. In addition, red blood cells scatter ultrasound poorly due to their relative acoustic impedance mismatch to plasma [21] resulting in the blood appearing dark on B-mode images [22]. Many approaches and new techniques

Table 1
Comparison overview between circulatory bubble types found in the bloodstream.

|	Approx. diameter (μm)	Gas content	Shell properties	Persistence in the bloodstream
Decompression bubble	Debated. The detectable VGE size using linear B-mode ultrasound is above 20–30 μm [13,14]. Theoretical predictions calculate bubbles of more than 5–10 μm [15]. Animal studies have observed 19–700 μm [16].	Inert gas breathed mainly (nitrogen usually)	Unknown, would depend on formation site	Observed circulating for up to 3 h post-dive using ultrasound imaging (supersaturated tissues state) [7]
Gas emboli from surgery [17,19]	Highly variable, 15–100 μm, slug form often observed	Ambient air of surgery room or anesthetic gas used	Unencapsulated	Depends on severity
Contrast agents for ultrasound and drug delivery bubbles [20]	1–7 μm	Usually heavy gas such as perfluorocarbon	Encapsulated (lipid or protein). Can have functionalized shell to attach to particular sites or carry drugs/DNA	Microbubbles remain for several minutes in the bloodstream enhancing contrast, but bubbles can remain in the body longer (accumulate in spleen and liver over 30 min)
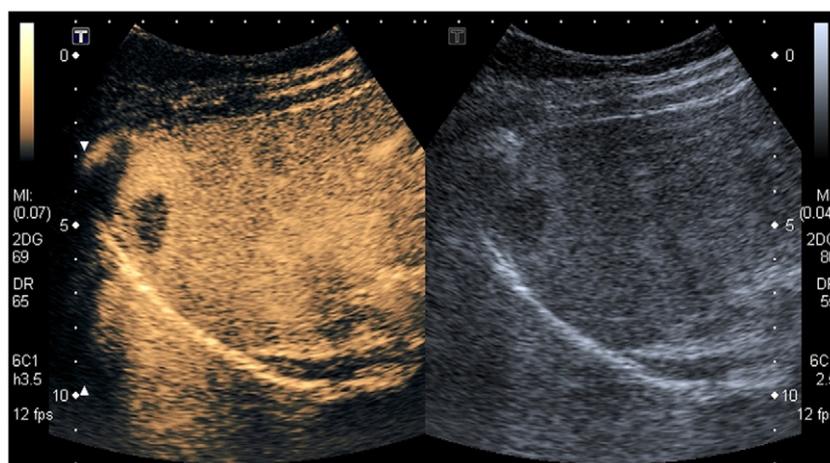
Fig. 1. Ultrasound imaging of a human liver with microbubble contrast agents: non-linear mode preferentially showing bubbles (left) and standard linear B-mode image (right).

are being developed to overcome some of the challenges related to ultrasound imaging, one of the most important being the development of stabilized gas microbubbles injected intravenously for enhancing the echogenicity from within the blood (contrast agent) [23]. These microbubbles of diameter less than 10 μm oscillate radially when hit by the pressure waves from ultrasound imaging and scatter those in all directions, thus increasing the contrast of the image drastically by effectively acting as secondary "point" sources of sound themselves (Fig. 1). Their scattering power is very big due to the large impedance difference between their gas core and the surrounding liquid and they can be driven at their resonant frequency for big radial amplitude oscillations. These microbubbles are encapsulated to last longer in the blood circulation, as free bubbles dissolve quickly [23], and so that they do not coalesce (e.g. PEGs on the shell). Acoustic signals from ultrasound contrast agents can be separated from those of tissue due to the fact that bubbles' non-linear response is much higher than that of soft tissues [24], making perfusion imaging possible.

The encapsulating layer of the microbubbles (protein or lipid) can be bound to molecules that attach to specific target sites in the body, for instance antibody, receptor or ligand of a cancer cell type or inflamed endothelium, etc. (Fig. 2). By functionalizing their shell, microbubbles can therefore be used for molecular imaging. In addition, microbubbles can be loaded with therapeutic agents or with DNA and act respectively as drug or gene delivery agents to specific target sites [25]. Primary and secondary ultrasound radiation forces, due to the incident pressure field and scattering by resonating bubbles respectively, can be used to push injected microbubbles towards their target sites and increase their chances of binding. It has also been demonstrated that the oscillation of bubbles next to cells under focused ultrasound field can open up cell membranes for delivery of therapeutic agents [26].

2.2. Unwanted bubbles in the bloodstream

Bubbles can form from micronuclei as a result of ultrasonic cavitation at high exposures [27]. Bubbles have also been shown to be created by cavitation where prosthetic heart valves move by disturbance of the normal flow at closure [28,29], with instances of up to 620 embolic events over 30 min recorded in patients [18]. Another iatrogenic cause of gas embolism is from surgery, where air is introduced in the vasculature during injections, catheter placing, etc. These bubbles can then be associated with all the serious clinical complications related to gas embolism, including ischemia, stroke and cardiac failure. Iatrogenic gas embolism is estimated to occur in only 2.65 per 100 000 hospitalizations, but with high long-term mortality and morbidity [30]. Gas embolism as a result of cardiopulmonary bypass for instance is estimated to result in cognitive decline consistent with cerebrovascular embolization restricting blood flow into localized areas of the brain for 25% of patients [31,33]. Seventy to eighty percent of strokes, the second leading cause of
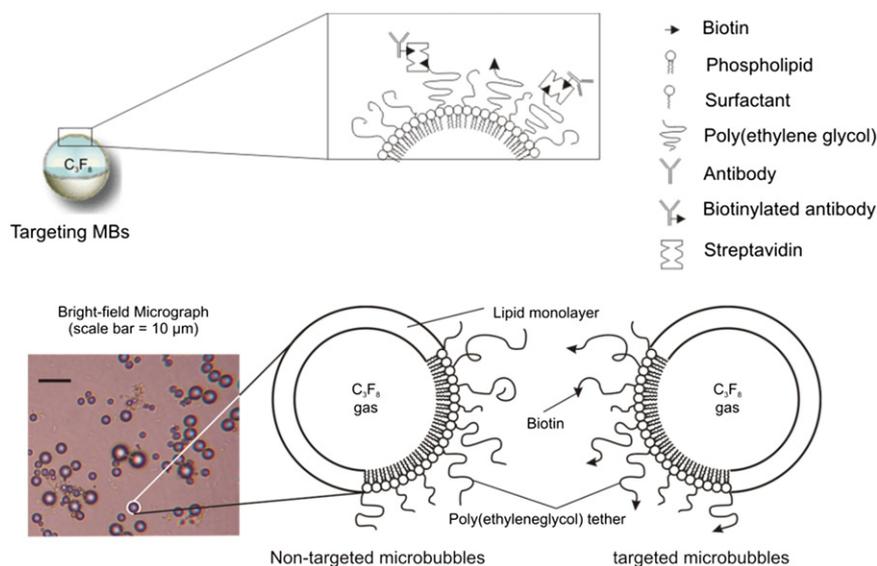

Fig. 2. Diagram of targeted microbubble shell composition.

death worldwide [34], are ischemic in origin, resulting directly from cerebral thrombosis or embolism blocking an artery in the brain or in the neck [35].

In addition, microbubbles can grow in the body due to changes in ambient pressure (scuba diving, extravehicular excursions for astronauts, etc.). The precise formation mechanism and site of these bubbles are still debated and the subject of a previous publication [7]: Potential stabilizing mechanisms for micronuclei from which bubbles can grow are hydrophobicity of surfaces and tissue elasticity, with formation sites in facilitating regions with surfactants, hydrophobic surfaces or crevices, such as caveolae or between endothelial cells. Intravascular bubbles post pressure-excursions are routinely observed with Doppler and B-mode ultrasound imaging. Human blood and tissue contain dissolved inert gases from respiration and cell metabolism, the molar concentrations of which are proportional to the gas partial pressure (Henry's law). The partial pressure of inert gases breathed is increased during a scuba diving descent, where the diver is supplied with air at ambient pressure throughout the dive (the ambient pressure at depth increases by roughly 1 atm for every 10 meter depth). This results in inert gases, not utilized by the body, being absorbed by tissues and blood during the descent phase of the dive. Metabolic gases, oxygen bound for the most part by hemoglobin, and carbon dioxide, do not cause problems as they are directly used by the body and recycled through breathing. Bubbles can grow during or after the decompression phase of the dive (ascent), when the inert gas (nitrogen and/or helium usually) that has been dissolved in the tissues during the compression phase (descent), is released in the circulation (Fig. 3). The tissues are then supersaturated and release inert gases in the form of in situ tissue bubbles or bubbles that form in, or enter, the bloodstream. Circulating bubbles are normally filtered out by the lungs (expiration) [36] and do not pass into the arterial side of the circulation, provided that they are big enough to be trapped and dissolved but small enough not to obstruct any vessels upstream of the lungs, and that their number does not impair the lung capability to filter them out. Failure to ascend slowly enough (following decompression stops where the diver waits at certain depths before resuming his ascent) to control the number and size of those bubbles can result in potentially fatal decompression sickness. In addition, the presence of venous-arterial shunts (cardiac PFO [37,38], lung shunts [39], …) can provide paradoxical entry for these bubbles into the arterial side of the circulation [37]. This effectively results in arterial gas embolism with the added complication of the body being more saturated in inert gas, which hinders bubble dissolution.
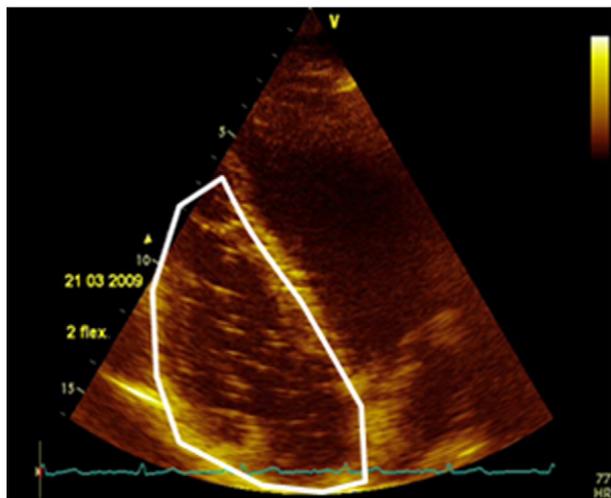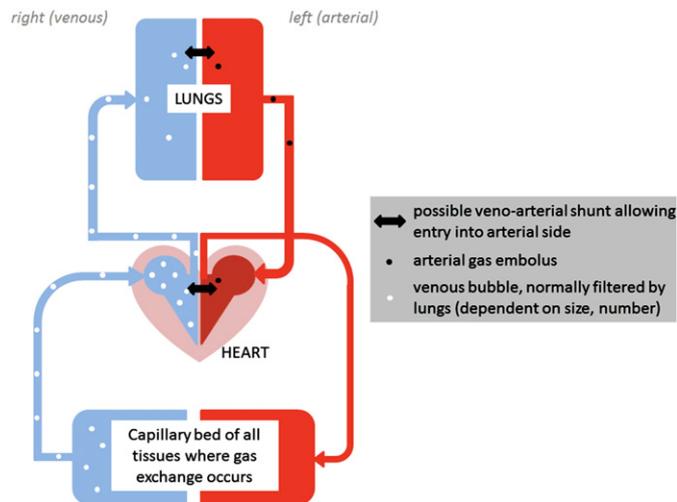

Fig. 4. Schematic of bubbles from decompression in the circulation.

2.3. Life cycle of a bubble in blood

Once a bubble has entered the bloodstream, let's assume on the venous side, if its size is small enough not to directly occlude a vessel it will be transported by the blood and follow the normal circulation into the right heart and then the lungs. The bubble will travel at the velocity of blood provided it is small compared to the vessel cross-sectional area, with velocities from 0.03 cm/s in the capillaries to 40 cm/s in the aorta and 15 cm/s in the vena cavae [40]. Microbubbles arriving in the lung capillaries are normally trapped if big enough, then dissolved during expiration [36].

In addition to a direct entry into the arterial side of the circulation, bubbles originally from the venous side can gain paradoxical entry into the arterial circulation in the presence of cardiac or pulmonary shunts (Fig. 4). A patent foramen ovale or PFO is one such venous-arterial shunt located in the atrial septum of the heart, with estimated prevalence in the population of 25–33% [37,38]. Another is intrapulmonary arterial-venous anastamoses (IPAVA) which allow blood to bypass the pulmonary microcirculation [39]. Both of these shunting mechanisms have been shown to be exacerbated by exercise [39] and provoking mechanisms that increase the intra-thoracic pressure [37,38].

Finally, bubbles can also enter the arterial circulation if the lung does not act as an efficient filter. It was shown in dog experiments that this can happen if the bubbles are too small to get trapped (less than 22 µm [36]) or if there are too many bubbles causing a deformation or rupture of the lung capillaries (administration of single bolus over 20 ml of gas [36] or 0.15 ml/kg·min for over 30 min [41]). Once a bubble is in the arterial side of the circulation the probability of it blocking the circulation increases as, conversely to the venous side of the circulation, the blood is transported into progressively smaller vessels and capillaries. This is especially the case if the bubbles continue to grow by merging into one another or due to the continued ascent and degassing in scuba diving.

Depending on the saturation dynamics of the rest of the blood and tissues, the bubble may dissolve or expand accordingly during transport. In any case the inflammation cascade initiates as the bubble persists in the circulation and gets in contact with other blood cells suspended in plasma or brushes against endothelial cells [42]. There is also evidence of macrophages internalizing bubbles and bubbles accumulating in the liver and spleen before the gas eventually diffuses out [43]. This is described in more detail in Biological interactions (Section 4.4).

Fig. 3. Ultrasound imaging of the heart 1 h post scuba dive. Venous gas emboli (VGE) are circulating in the right heart chambers (delimited in white, image reversed). The lungs are effectively filtering these VGE and they do not appear in the left heart chambers.

3. Bubble growth and detachment from decompression

Notwithstanding chemical interactions, a supersaturated state can be reached in a liquid solvent containing dissolved gas as a result of a reduction in ambient pressure or rise in liquid temperature. Above a respective critical supersaturation level, gas bubbles will nucleate heterogeneously or homogenously. The rate of gas desorption from the liquid therefore is associated with both the nucleation and the subsequent growth rates of those bubbles once formed, as well as their detachment rate. While bubble growth is primarily linked to gas mass transfer from the bulk liquid to a gas nucleus, bubble detachment is dictated by buoyancy and/or flow induced shear forces which both act to destabilize the bubble contact with the solid surface beneath and drag it away from its nucleation site [44].

In the absence of pre-existing small bubbles or gas cavities (micronuclei), homogeneous bubble nucleation requires very high levels of supersaturation [7,45]. Heterogeneous nucleation is therefore most likely at play, facilitated by either cavities and different materials in the liquid or pre-existing gas cavities triggered to growth [7]. Accounting for the stability of these pre-existing nuclei is reviewed in a previous publication [7]. Here we are focusing on the description for their subsequent growth and detachment in the bloodstream.

Bubble growth in the bloodstream can be induced by different mechanisms related to heat and/or pressure. These range from the flow conditions in the circulation to the oscillations induced by ultrasound imaging of bubbles (changing pressure and heat of contrast agent bubbles). In the case of interest here we consider the ambient pressure changes as the main driving force of growth: a rapid or gradual, staged or continuous, pressure decrease (decompression) in solutions with dissolved gas as an analog to the case of the bubbles observed in blood in scuba divers for instance.

3.1. General formalism: heat and mass transfer

A small gas bubble which has nucleated on a solid surface in contact with a liquid containing this dissolved gas can grow and finally detach from it [46]. The description of the growth rate of the bubble requires the coupling of the equations of motion, continuity, conservation of diffusing species and heat transfer, and must account for convection, viscous and surface tension forces, as well as other flow conditions [44,45,47].

In the simple case with no flow (basin degassing) at constant temperature, after the initial growth phase, the growth of the bubble will be theoretically governed by molecular diffusion with a scaling relationship of the form $R \sim t^a$, where R is the bubble radius, t the time of growth and a the scaling factor [48,49]. However the range of scaling factors a was obtained experimentally and values differ not only between classes of problems, but also for the same type of experiments [44,45,48]. The difficulty comes from devising experiments to test the theoretical predictions, as it is very difficult to decouple heat and mass transfer in experiments, for instance to get a decompression driven bubble growth at constant temperature.

In general bubble growth can be separated into two categories depending on the driving force [50]: bubble growth that is primarily controlled either thermally [47,51,52] or inertially (mass transfer) [53] such as in the decompression case.

We review below the basic considerations for the heat diffusion case, before treating in more detail the bubble growth resulting from decompression of a liquid containing dissolved gas in Section 3.2.

3.2. Thermal degassing (heat transfer controlled)

Scriven [52] derived the influence of radial convection on bubble growth from molecular diffusion of the gas molecules through the liquid and the liquid–gas interface. The outward convective movement of the growing bubble front is shown to result in an effective higher molecular

diffusion and thus an increase in growth rate than that expected from diffusion considerations alone:

$$R = 2b\sqrt{kt}, \tag{1}$$

where R is the bubble radius, t growth time, b a dimensionless growth constant and k a diffusion term. In the case of heat conduction governed growth, k is the thermal diffusivity, and for growth governed my molecular diffusion k is the diffusivity. Eq. (1) shows that the radius is proportional to the square root of time for a negligible Laplace pressure. The bubble growth constant β was also explicitly related to the densities and concentrations of gas and liquid through a dimensionless superheat or supersaturation parameter

$$\varphi = \varphi\{\varepsilon, b\} = \frac{\rho_L(C_0 - C_{sat})}{\rho_G(\rho_L - C_{sat})}, \tag{2}$$

with

$$\varepsilon = 1 - \frac{\rho_G}{\rho_L}, \tag{3}$$

where ρ_G and ρ_L are the densities of the gas and liquid respectively, and C_0 and C_{sat} the mass based concentrations of the bulk and equilibrium concentrations of the gas in the liquid.

The above 1D analysis has been extended to include temperature dependent transport properties of the liquid and the gas as well as a 2D description of bubble growth and motion on a non-flat surface [44,48].

3.3. Decompression degassing (mass transfer controlled)

3.3.1. Pool degassing (diffusion controlled)

The desorption or release of the dissolved gas in a fluid brought to supersaturation can be done either solely by diffusion through the liquid contact area to the air for instance or in a nucleating fashion, in other words through the formation of bubbles. In the latter case, desorption is not simply the analog of the absorption kinetics and the diffusive mass transfer equations are significantly altered by the hydrodynamic conditions in the liquid.

Desorption without bubble creation has been examined [54,55], however the case of desorption with bubble formation has rarely been considered [56]. For these, a first factor must be the availability of nucleation sites for the bubbles to form due to small pressure ratio reductions. For quiescent solutions (no flow), the conditions under which the bubbling degassing mechanism dominates over normal diffusive mechanisms were first investigated by Schweitzer et al. [57] and Burrows et al. [58], showing that bubbles could be prevented if the pressure reduction rate was slow enough for total pressure reduction ratios of up to 3.75. It is, of course, expected that if the ambient pressure is below the sum of partial pressures of the solute and solvent, then under isothermal conditions at constant volume the system will tend to reinstate pressure equalities by gas and vapor evolution [55].

Isothermal bubble growth from capillary effects, inertia, viscosity and mass diffusion of a solute gas from a liquid was investigated theoretically by Langlois [59]. Neglecting the inertia of the liquid, the radius of the bubble was shown to satisfy

$$\frac{4\mu_L}{R}\frac{dR}{dt} + \frac{2\sigma_L}{R} = AC_{sat} + \frac{p_{g0}R_0^3}{R^3} - P_{amb}, \tag{4}$$

where R is the bubble radius, R_0 the initial bubble radius, μ_L the viscosity of the liquid, σ_L the surface tension of the liquid, P_{amb} the ambient pressure, p_{g0} the initial partial pressure and C_{sat} the concentration of solute gas related by Boyle's law to its partial pressure such that $p_g = AC_{sat}$ with A being a constant.

Once formed, the general growth and dissolution of microbubbles in a solution from diffusion considerations was derived by Epstein and Plesset [60]:

$$\frac{dR}{dT} = \frac{D_G BT / M_G (C_0 - C_{sat})}{P_{amb} + 4\sigma_B / 3R}\left(\frac{1}{R} + \frac{1}{\sqrt{\pi D_g t}}\right) \tag{5 - EP}$$

where R is the radius of the bubble, t time, D_G the gas mass diffusivity in the fluid, B the universal gas constant, M_G the molecular weight of the gas, C_0 the bulk dissolved gas concentration, C_{sat} the saturated concentration of the dissolved gas, P_{amb} the ambient pressure, σ_B the surface tension of the bubble and T the temperature. Eq. (5-EP) predicts that the bubble will dissolve for saturated solutions ($C_0 = C_{sat}$) if its surface tension $\sigma_B \neq 0$.

Eq. (5-EP) predicts a dissolution time for a perfectly spherical air bubble in pure water of 1 s for a 1 μm radius bubble, 1–6 s for a 10 μm bubble and 11–70 days for a 1 mm bubble [61]. However bubbles can take a cylindrical form in vivo, in which case the dissolution time for a bubble of same total volume is multiplied by a factor of at least 2 [61].

The Epstein–Plesset model was most comprehensively tested for the effects of surface tension and undersaturation recently using a new micromanipulation (micropipette) technique [62]. Surface tension was studied using single and double-chain surfactants and undersaturation coating the microbubble with a wax monolayer from solid distearoylphosphocholine lipid to effectively achieve a zero surface tension. The model was shown to underpredict the resolution time of microbubbles due to surface tension in the range of 72–25 nN/m by an average of 8.6% and overpredict this time due to undersaturation by 8.2% in the range of gas saturation from 70 to 100%.

3.3.2. Flow degassing (inertia controlled)

Fluid mechanics also play a role in the conditions for maintaining bubbling and we can consider either a basin/pool degassing scenario as treated above or a flowing liquid degassing for which calculations of desorption rates by mass transfer are even more limited [63].

The rate of gas desorption with bubble formation from agitated liquids was investigated using a stirred cell apparatus from CO_2 supersaturated aqueous solutions [55]. It was found that in a flow system considerable bubbling does not start until the partial pressure of the dissolved gas alone is greater than the ambient pressure, and only a minimal amount of bubble evolution occurs when the sum of partial pressures of the components of the liquid exceed the total pressure.

The same flat gas–liquid interface system was then studied in a continuously baffled agitated vessel and the rates of desorption of carbon dioxide and nitrogen from supersaturated water solutions measured at different temperatures to extract volumetric mass transfer coefficients for desorption and correlate those to the relative supersaturation of the solution and its Reynolds number [64].

In a more recent study, the volumetric mass transfer coefficients for the bubbling desorption of CO_2 from DMEPEG solutions were correlated by a power relationship to supersaturation, Reynolds and Weber numbers [63]. It therefore appears that the viscosity and surface tension of the fluid with respect to its inertia can be important quantities in addition to the degree of supersaturation.

3.4. Bubble detachment

3.4.1. In stagnant liquid

Let us consider the forces acting upon a bubble growing on a surface in a liquid. The forces that contribute to its adhesion to the surface are the surface tension F_S and drag produced by the bubble growth F_D, whereas the forces which pull it to detach are buoyancy F_B, pressure F_P and liquid inertial F_I forces [45]. So the force balance equation is

given by:

$$F_S + F_D = F_B + F_P + F_I, \tag{6}$$

which, for slow growth rates, simplifies to

$$F_S = F_B + F_P. \tag{7}$$

The time of detachment is a function of the contact angle of the bubble with the surface, the surface geometry itself, as well as the flow conditions. For bubbles growing from conical cavities, where the contact angle of the growing bubble is θ, at detachment the surface adhesion force is just balanced by the pressure and buoyancy forces, such that

$$2\pi R_d \sigma \sin\theta = \left(\frac{2\gamma}{R'} - \Delta\rho g H\right)\pi R_d^2 + \Delta\rho\sigma V, \tag{8}$$

where R_d is the radius of the bubble at detachment, H the bubble height, R' the radius of curvature of the bubble at its highest point, g the acceleration due to gravity, $\Delta\rho$ the mass density difference between the gas of the bubble and the fluid ($\Delta\rho \equiv \rho_G - \rho_L$), σ the interfacial tension between the fluid and the gas, and V the bubble volume.

Chappell et al. investigated the effect of the cavity geometry on growth rate and detachment [65,66], showing that once the bubble has emerged from the cavity its behavior is determined by the size of the opening. The flow conditions, not considered explicitly in this cavity geometry effect modeling, are expected to dictate the behavior for detachment much more than the cavity geometry after the initial bubble growth phase [61].

3.4.2. In flowing liquid

The ensemble of forces pulling the bubble upwards or lift force experienced by a bubble moving in the liquid flow can be much more complicated. For example in a non-symmetrical flow, the bubble experiences a lift force perpendicular to its plane of motion and many ad hoc expressions of the lift force are used in bubbly flows to reconcile the experimental observations [67]. Experiments in microgravity showed that bubbles tend to migrate towards the center of the pipe [68].

The bubble detachment criterion of a bubble growing at the wall of a linear shear viscous flow can be obtained from a force balance equation derived by Duhar et al. [69,70]:

$$F_c + F_{CP} + F_B - \int_{S_B}(P_L - P_{LZ0})\boldsymbol{n}\, dS + \int_{S_B}\boldsymbol{\tau}_L \boldsymbol{n}\, dS = \boldsymbol{0}, \tag{9}$$

with the capillary force F_C such that [71]

$$F_C = 1.25 \times 2r_C\sigma_L\frac{\pi(a-\beta)}{\pi^2 - (a-\beta)^2}(\sin a + \sin\beta)\boldsymbol{e_X} \tag{10}$$

$$- 2r_C\sigma_L\frac{\pi}{(a-\beta)}(\cos\beta - \cos a)\boldsymbol{e_Z},$$

the contact pressure F_{CP}

$$F_{CP} = \left(\frac{2\sigma_L}{R} - \rho_L g H\right)\pi r_C^2 \boldsymbol{e_Z}, \tag{11}$$

and the buoyancy force F_B encompassing both gravity and Archimedes forces

$$F_B = (\rho_G - \rho_L)\frac{4}{3}\pi R^3 \boldsymbol{g} \tag{12}$$

where S_B is the surface of the bubble, $\boldsymbol{n}$ the unit vector normal to the bubble surface, $\boldsymbol{g}$ the gravitational acceleration, ρ_G the bubble gas density, ρ_L the density of the liquid, P_L the pressure of the surrounding liquid, P_{LZ0} the reference pressure in the liquid at the wall (at $Z = 0$ with respect to Fig. 5), R the bubble radius, σ_L the surface tension of the liquid, r_C the
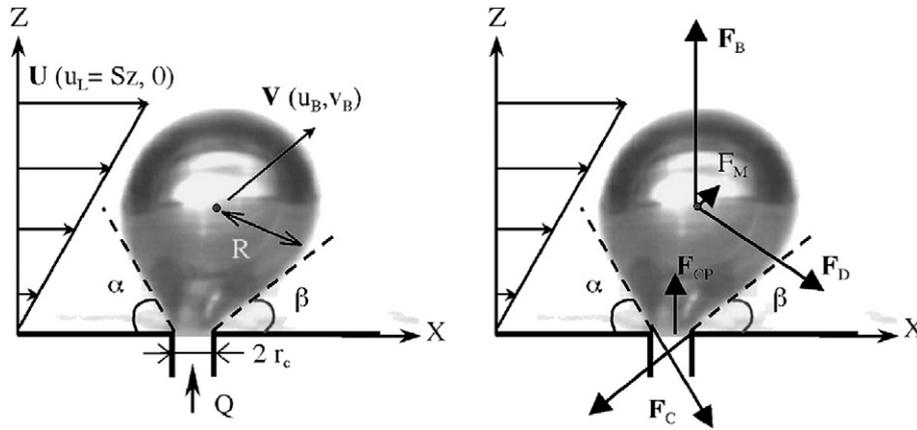
Fig. 5. Geometrical definitions of parameters for the velocities and force balance equations (figure from [66]).

orifice radius of the conical cavity from which the bubble grows, H the bubble height, a the advancing contact angle, β the receding contact angle, e_X the unit vector parallel to the wall, e_Z the unit vector perpendicular to the wall and τ_L the deviatoric stress tensor due to viscous effects.

The first 3 terms of Eq. (9) are the static forces and the last 2 terms the hydrodynamic forces encompassing the drag, migration and unsteady forces. The contact angles (Fig. 5) were shown to continuously evolve during growth and detachment occurs for maximum capillary force value of the advancing contact angle, 70° for a quiescent liquid and 90° in a shear flow. In addition, Duhar et al. [37] derived simplified departure radius equations (less than 5% error) for both the quiescent liquid and shear flow cases.

It remains however to be determined to which extent the above formulations apply to the case of bubbles in the bloodstream. The lack of information in this regard is no doubt due to the practical difficulty of observing bubble detachment from vessels in vivo, which would in addition require creating these bubbles and predicting their nucleation site. A first step in this direction was the recent demonstration ex-vivo of bubble formation on the surface of hydrophobic vessels [72]. We have also developed a set-up that permits the real-time observation of bubble growth rates and densities over surface area from hyperbaric decompression on ex-vivo tissues with an optical resolution of 1.75 μm [73].

Chappell et al. [74] modeled bubble detachment in blood for bubbles growing in cavities of the vessels' walls during decompression from a saturation dive. The detachment process was separated into two distinct phases: bubble deformation with the bubble growing deflected sideways in the direction of the flow but still attached to the cavity mouth and assumed approximately spherical, then detachment once the bubble separated from the cavity. The detachment happens when the drag force experienced by the bubble due to the blood flow exceeds the capillary force. Assuming that the flow around the spherical bubble is laminar (Reynolds number ~0.001) and that the variation ψ of contact angles a and β is symmetrical a force balance between the drag and capillary forces gives

$$\psi = \frac{6\mu_L}{\sigma_L}\left(\frac{R'}{r_C}\right)^2, \tag{13}$$

where μ_L is the blood viscosity, σ_L the surface tension, r_C the radius of the crevice mouth and R' the radius of curvature of the bubble. The limiting value of deformation angle ψ_{crit} is then used to get the non-dimensional radius of the bubble at the end of the deformation phase, R'_{crit}/R, by rearranging Eq. (13) to get R'_{crit}.

4. Bubble behavior in the bloodstream

4.1. Bubble dissolution in blood

In the case of decompression bubbles growing in tissue or blood, assumed liquid for simplicity, the nucleation and subsequent growth of decompression bubbles is dependent on the dissolved gas content (concentration and diffusivity). The solubility and mass diffusivity of different inert gases (commonly nitrogen and helium in scuba diving) are not identical and influence bubble dynamics. Experimental values for diffusion and solubility coefficients for gases in biological tissues and fluids are scarce and reviewed in [75]. It is estimated [75] that diffusion coefficients in tissues are 25% to 50% lower than for water and that the solubility coefficients for water can be used as an approximation (less than 20% error) for most tissues apart from fat tissues which have higher coefficients.

Once formed a gas nuclei (bubble of at least the critical radius size to avoid dissolution due to surface tension effects etc.) will tend to equilibrate the differences between the dissolved gas tension in the liquid and the bubble gas pressure at its interface.

The Epstein–Plesset Eq. (5-EP) presented in Section 3.3.1 was adapted for multi-component bubbles without encapsulation in blood by Kabalnov et al. [76]:

$$\frac{dR}{dt} = -D_G L_G \frac{p_{exc} + 2\sigma_B/R}{P_{amb} + 4\sigma_B/3R}\left(\frac{1}{R} + \frac{1}{\sqrt{\pi D_G t}}\right). \tag{14}$$

Where D_G is the gas diffusivity, L_G the partition coefficient of the gas between the liquid phase and the bubble and p_{exc} the excess pressure (sum of excess systemic blood pressure with excess partial pressure of the dissolved gases from the atmosphere to the bloodstream).

The evolution of bubbles in supersaturated tissue is particularly relevant to DCS and was investigated theoretically by Srinivasan et al. [77,78] using a modification of the Epstein and Plesset model with three regions (bubble inside tissue mass but separated from it by an unstirred boundary layer of constant thickness).

The detachment model developed by Chappell et al. [74] calculated the possibility of a gas plug directly occluding the capillary in which the bubble forms after the dive from the distance traveled by the bubble laterally, assuming the bubble travels at the same speed as blood flow velocity. The gas concentration in the fluid (blood) was assumed to change much slower than the gas transfers into the bubble, with a boundary layer of finite thickness and varying gas concentration around the bubble. It was shown that a bubble growing after a dive could theoretically create a gas plug directly in the capillary where it originated, although vessel deformation and interaction of the bubble with the flow field were not considered.

The physiological concept of the oxygen window, or inherent unsaturation due to oxygen metabolism [79], was used by Van Liew and Burkard [80] to explain how stabilized microbubbles can persist in the bloodstream. This was done simply by equating the pressure on the bubble surface to the sum of the partial pressures of gases inside the bubble. They also suggested that gases inside the bubble can be at diffusion equilibrium if the bubble is able to support some degree of negative pressure mechanically.

Looking at bubble dissolution, the extravascular bubble model by Van Liew [81] was applied to the circulating bubble [82]. The supersaturation state of the mixed venous blood during decompression means that the bubbles will dissolve slower or even expand, potentially resulting in a lung filter overload.

A mathematical model to account for the cylindrical geometry of bubbles observed in vivo was also developed [83], showing that the absorption time observed corresponded better to the predictions of the model. Once the length of the cylindrical bubble has shrunk, it reduces to a spherical geometry and any subsequent shrinkage will decrease its diameter. This geometry results in longer absorption times than expected for spherical bubbles, as observed with gas emboli in vivo [83,84]. A similar model using this in vivo bubble geometry in vessels was developed for use in hyperbaric oxygen treatment, to determine the most effective treatment protocols for cerebral gas embolism [85].

Finally, the intravascular exogenous surfactant concentration was not found to influence initial bubble conformation, but increased bubble breakup and the rate of bubble reabsorption [86]. In an in vivo rat model of cerebrovascular arterial gas embolism, intravenously injecting them with a surfactant prior to inducing cerebral gas embolism showed a prophylactic effect: strokes were undetectable on brain MRI scans and post embolic cognitive and sensorimotor deficits were significantly reduced [87].

4.2. Bubble dynamics in an ultrasound field

The equations for microbubbles in an ultrasound field are mostly modifications of the Rayleigh–Plesset equation [88,89] describing the dynamics of a free perfectly spherical bubble surrounded by an unbounded viscous incompressible liquid in the far-field $P_\infty(t)$ at constant liquid temperature and uniform pressure in the bubble $P_B(R)$:

$$\rho_L\left[R\frac{d^2R}{dt^2} + \frac{3}{2}\left(\frac{dR}{dt}\right)^2\right] + \frac{4\mu_L}{R}\frac{dR}{dt} + \frac{2\sigma_B}{R} = P_B(R) - P_\infty(t), \quad (15)$$

where μ_L and ρ_L are respectively the viscosity and density of the liquid and σ_B the surface tension of the bubble of radius R.

Assuming that the vapor pressure in the bubble and non-linear terms are negligible and that the pressure field far from the bubble changes sinusoidally [89],

$$P_B(R) = P_G(R) = P_{Geq}\left(\frac{R_0}{R}\right)^{3\gamma}; \quad P_{Geq} = P_{eq} + \frac{2\sigma_B}{R_0}; \quad (16)$$

$$P_\infty(t) = P_{eq} - P_A\sin(\Omega t),$$

the radial oscillatory behavior of the bubbles can be derived by approximating a first-order solution to this equation as

$$R \approx R_1(t) = \frac{A_{1r}(\Omega)}{2}P_A\exp(i\Omega t), \quad (17)$$

where the subscript *eq* refers to the quantity at equilibrium, P_A is the pressure amplitude and $A1r(\Omega)$ the linear amplitude–frequency response of the bubble which depends on the liquid density and viscosity, the gas pressure (or sum of partial pressures of gases) in the bubble P_G, the adiabatic exponent γ (ratio of the heat capacity at constant pressure to heat capacity at constant volume for the gas mixture) and the angular transmitted frequency $\Omega = 2\pi f$ with f the frequency of bubble oscillation. The full derivation and explicit equations for the linear amplitude–frequency of the bubble response $A1r(\Omega)$ can be found in [90,91].

Some of the effects that are not taken into account in Eq. (15) are the heat conduction and gas diffusion through the bubble wall, the blood composition making compressibility of the fluid and viscoelasticity effects potentially important, the shell effect, as well as the interactions between the bubbles and the blood cells and endothelial boundaries.

For small radial oscillations, corrections to Eq. (15) have been developed to this effect [92,93], which led to the de Jong models assuming that the shell of the bubbles dominates their response [94,95]. However Sboros et al. [96] showed that the behavior of those bubbles is not compatible with the theoretical predictions of the viscoelastic ball model of de Jong. Another theoretical model for an encapsulated bubble was suggested by Church [97] who considered a finite thickness for the shell, separating the interface of the bubble into two layers of different surface tension to reflect the different boundaries with gas and liquid respectively. In addition, a complicating factor of the modeling is the fact that oscillating bubbles do not always remain spherical in shape [19] and are clearly asymmetric near the vessel walls [98].

An important consequence of Eq. (15) is that over time the oscillating bubble near resonance can be growing due to rectified diffusion [99]. The diffusion rate of gas into the bubble is indeed proportional to its surface area and therefore the net effect of oscillations will be to grow the bubble over each oscillation cycle. It has been shown that the effect of rectified diffusion is accelerated in the presence of surfactants at the bubble-liquid boundary [17].

4.3. Rheology of microbubbles in the bloodstream

4.3.1. Brief overview of blood rheology

Blood plasma can be approximated to a Newtonian liquid [100] in the case of studies involving microbubbles in arteries or in vitro conditions in an ultrasound field. This is because viscoelastic effects (due to blood cell deformation and vessel walls) can be ignored if the bubble is growing more than 25 bubble radii away from the vessel walls [101]. However for bubbles in small veins and capillaries, as well as those growing in tissue, this is not the case and those cannot be modeled as simple Newtonian fluids [102].

Blood is a mixture of suspended red blood cells, white blood cells and platelets in plasma. Plasma contains mainly water and proteins and lipids, and is a Newtonian fluid, i.e. its shear stress is linear with the strain rate [103]. The non-Newtonian rheology exhibited by blood is down to the cellular components. When these are small compared to the diameter of the vessel, this effect can be ignored and blood is approximated to a continuum. For an incompressible Newtonian fluid, the conservation of fluid mass and that of linear momentum yield the following equations respectively [104]:

$$\nabla \cdot \boldsymbol{u} = 0, \quad (18)$$

and

$$\rho_L\left(\frac{\partial \boldsymbol{u}}{\partial t} + (\boldsymbol{u}\cdot\nabla)\boldsymbol{u}\right) = -\nabla P + \mu_L\nabla^2\boldsymbol{u} + \rho_L\boldsymbol{g}, \quad (19)$$

where ρ_L is the fluid density, $\boldsymbol{g}$ the acceleration due to gravity, $\boldsymbol{u}$ the velocity vector, P the pressure, and μ_L the fluid viscosity. For non-Newtonian fluids, the shear stress term in Eq. (19) is changed to reflect the shear-stress relationship for that fluid.

Over a range of shear stresses which depend on its hematocrit content, blood is a shear thinning fluid, i.e. its viscosity decreases with an increasing strain rate. Below a critical *yield stress* value of shear stress [103], blood does not behave like a viscoelastic fluid anymore, but like a solid. A constant effective fluid viscosity can be implemented, or the

non-Newtonian properties of blood can be approximated by the Casson model [103]. For blood flow in the capillaries, the diameter of the red blood cells is similar to that of the vessel and they have to deform and go through one at a time in a file, so the continuum approximation is not valid [105,107].

Eqs. (18) and (19) are subject to boundary conditions to account for the circulation of blood from one region of flow to the other (continuum) and also for the wall condition (elasticity etc.). Blood flow in the arteries is generally pulsatile, whereas it is nearly steady in capillaries and veins [108,109].

It is therefore clear from the brief overview above that different forces resulting from these flow conditions can act upon the bubbles, thus giving different bubble behavior.

4.3.2. Interfacial tension and surfactants

The interfacial tension, or force per unit length along the interface between the gas phase present due to bubbles and the fluid that is blood, has to be considered [104]. The Young–Laplace law relates the pressure discontinuity ΔP across the interface assumed static, to the mean interfacial curvature κ, and interfacial tension σ [110]:

$$\Delta P = 2\sigma\kappa. \tag{20}$$

For a dynamic interface, this equation is replaced by:

$$\Delta \boldsymbol{f} = \sigma\kappa\boldsymbol{n} + \nabla_S\sigma, \tag{21}$$

where ∇_S is the surface gradient operator, $\boldsymbol{n}$ the normal unit vector and $\boldsymbol{f}$ the traction at the boundary such that $\boldsymbol{f} = \boldsymbol{\sigma} \cdot \boldsymbol{n}$ with $\boldsymbol{\sigma}$ the stress tensor [110]. For a Newtonian fluid, the normal stress discontinuity is balanced by the interfacial curvature term and the tangential stress discontinuity by the interfacial tension gradient. Due to boundary conditions, interface position $\boldsymbol{Y}$ follows

$$\frac{\partial \boldsymbol{Y}}{\partial x} \cdot \boldsymbol{n} = \boldsymbol{u} \cdot \boldsymbol{n} \tag{22}$$

meaning that the interface moves at the velocity of the normal component of the fluid at the interface. As the bubble starts to move and deform with the flow, the interface position becomes part of a moving boundary problem since the dynamics of the interface and fluid are coupled. The interfacial tension σ is typically constant for a clean interface with no temperature differences, but depends on the interfacial surfactant concentration when surfactants are present. If there is a gradient in surfactant concentration on the boundary, then this results in a shear stress gradient along the boundary, inducing Marangoni flows [104]. Surfactants or surface active species can therefore affect the dynamics of cardiovascular bubbles [111]. In blood there are many lipids and proteins that are surface active which are soluble in blood and transported by convection and diffusion [112,113].

4.4. Biological interactions

Bubbles which are formed in vivo or introduced in the organism interact with living cells. In addition to the purely mechanical implications, there induce a variety of biochemical responses. Interaction between bubbles and blood [114,115], endothelial damage, and microcirculatory impairment [116] have all been shown.

Nevertheless studying this phenomenon precisely is difficult. Studies in vitro and ex-vivo, although insightful, are difficult to extrapolate to living cells in their complex environment. The main limitation of animal studies, on the other hand, is the higher complexity level that humans exhibit and the inability to isolate phenomena for study. There are also practical difficulties in finding adequate transparent tissue for intravital microscopy of microbubbles in blood vessels [117]. Computational and analytical studies can fill the gap between these methodologies to a

certain extent; however the inflammation cascade caused by bubbles is an additional important problem to consider.

Not considering the disruption that bubbles may cause to get into the circulation in certain cases, once the bubbles have detached and are flowing in the vasculature their effect on endothelial function has to be questioned. It was found in the case of microbubbles injected in excised rat vessels for instance that their adhesion to the endothelium is significantly lowered in the presence of surfactants [118]. This could be due to surfactants acting as drag-reducing agents [119,120] and reducing shear forces so that the mechanical stress upon the endothelial surface is reduced. Adhesion of microbubbles to endothelial cells, as well as damage to these, may trigger an inflammatory response and obstruct blood flow, causing ischemic injuries [121]. The properties of the bubble boundary layer are clearly relevant to characterize adhesion properties.

It has been shown for instance that some circulating molecules or dissolved substances in blood can adsorb on interfacial area of the bubble altering their dynamic behavior [122,124]. Proteins adhering to the bubble interface can affect the adhesion interaction to endothelial cells [6,83,125]. In addition, they can play a role in signaling clot formation [112]. The adhesion of gas emboli to the endothelial surface was thus shown to result from the blood-borne macromolecules attached to the bubble surface [6]. These considerations are important for the therapy of gas embolism, as it has been suggested that adding surfactants to the perfusate can reduce bubble adhesion force [126].

Nitrogen bubbles have also been observed to induce an inflammatory response. Platelets and leucocytes have been shown to aggregate with the presence of bubbles [127,128], denature lipoproteins and activate complement, bradykinin and coagulation systems [42]. These in turn induce capillary leakiness and hemoconcentration [129,130], which contributes to the difficulty of treating decompression sickness by means of recompression only once this inflammatory process is under way.

Ultrasound contrast agents can also be internalized by cells. For instance various contrast agent types have been shown to be phagocytosed by Kupffer cells (liver-specific macrophages) in vitro [131]. The fact that some bubbles therefore end up accumulating in the liver or spleen can be used for delayed phase imaging [43].

5. Conclusion

Bubble growth from desorption of a liquid containing dissolved gas is generally dependent on both heat and mass transfer. The case of decompression driven growth primarily dependent on mass transfer was presented for the bubbles growing endogenously in the body of scuba divers during and after their ascent from a dive. This decompression degassing was separated into the diffusion and inertia controlled bubble growth from a pool or flowing liquid respectively. The detachment equations for a bubble growing on a solid surface in a liquid were then presented with and without flow. The behavior of bubbles in the bloodstream was considered, looking in particular at their time to dissolution under different saturation conditions and geometries, rheology and biological interactions.

Defining the exact cut-off point between the presence of bubbles in the circulation and the observation of clinical symptoms is yet unclear, in both the endogenously formed bubble case from decompression [34] or mechanical heart valves [132] and the iatrogenically introduced bubbles [5]. The persistence of bubbles in the bloodstream is crucial in these inflammatory processes and gas composition of the bubbles compared to the dissolved gases in the body affects the elimination time, therefore the solubility and diffusion coefficients of these gases in the given tissues are of interest [75]. As such, physical modeling and imaging techniques that can offer estimates of numbers and sizes of bubbles, as well as shell properties information, are clearly needed. Indeed the rheological behavior and interaction of bubbles with the different

components of blood and vascular wall determine the inflammatory response triggered and ultimately the clinical presentation.

Acknowledgments

References

[1] Arefmanesh A, Advani SG, Michaelides EE. An accurate numerical-solution for mass diffusion-induced bubble-growth in viscous-liquids containing limited dissolved-gas. Int J Heat Mass Transf 1992;35:1711–22.

[2] Payvar P. Mass transfer-controlled bubble-growth during rapid decompression of a liquid. Int J Heat Mass Transf 1987;30:699–706.

[3] Yoo HJ, Han CD. Oscillatory behavior of a gas bubble growing (or collapsing) in viscoelastic liquids. AIChE J 1982;28:1002–9.

[4] Edzwald JK, Malley JP, Yu C. A conceptual-model for dissolved air flotation in water-treatment. Water Supply 1991;9(1):141–50.

[5] Muth CM, Shank ES. Gas embolism. N Engl J Med 2000;342:476–82.

[6] Suzuki A, Eckmann DM. Embolism bubble adhesion force in excised perfused microvessels. Anesthesiology 2003;99:400–8.

[7] Papadopoulou V, Eckersley RJ, Balestra C, Karapantsios TD, Tang MX. A critical review of physiological bubble formation in hyperbaric decompression. Adv Colloid Interface Sci 2013;191–192:22–30.

[8] Poland MP, Sutton AJ, Gerlach TM. Magma degassing triggered by static decompression at Kilauea Volcano, Hawai'i. Geophys Res Lett 2009;36.

[9] Lensky NG, Navon O, Lyakhovsky V. Bubble growth during decompression of magma: experimental and theoretical investigation. J Volcanol Geoth Res 2004;129:7–22.

[10] Gardner JE, Hilton M, Carroll MR. Bubble growth in highly viscous silicate melts during continuous decompression from high pressure. Geochim Cosmochim Acta 2000;64:1473–83.

[11] Zehner P, Benfer R. Modelling fluid dynamics in multiphase reactors. Chem Eng Sci 1996;51:1735–44.

[12] Heide K, Hartmann E, Stelzner T, Muller R. Degassing of a cordierite glass melt during nucleation and crystallization. Thermochim Acta 1996;280:243–50.

[13] Hills BA, Grulke DC. Evaluation of ultrasonic bubble detectors in vitro using calibrated microbubbles at selected velocities. Ultrasonics 1975;13:181–4.

[14] Lubbers J, Van Den Berg JW. An ultrasonic detector for microgasemboli in a bloodflow line. Ultrasound Med Biol 1977;2:301–10.

[15] Van Liew HD, Conkin J, Burkard ME. How big are decompression-sickness bubbles? Proceedings of the XIXth Annual Meeting of European Undersea Biomedical Society. Trondheim, Norway: SINTEF Unimed; 1993 258–62.

[16] Hills BA, Butler BD. Size distribution of intravascular air emboli produced by decompression. Undersea Biomed Res 1981;8:163–70.

[17] Lee J, Kentish S, Ashokkumar M. Effect of surfactants on the rate of growth of an air bubble by rectified diffusion. J Phys Chem B 2005;109:14595–8.

[18] Pugsley W, Klinger L, Paschalis C, Treasure T, Harrison M, Newman S. The impact of microemboli during cardiopulmonary bypass on neuropsychological functioning. Stroke 1994;25:1393–9.

[19] Tian Y, Ketterling JA, Apfel RE. Direct observation of microbubble oscillations. J Acoust Soc Am 1996;100:3976–8.

[20] Cosgrove D. Ultrasound contrast agents: an overview. Eur J Radiol 2006; 60:324–30.

[21] Mast TD. Empirical relationships between acoustic parameters in human soft tissues. Acoust Res Lett Online 2000;1:37–42.

[22] Stewart MJ. Contrast echocardiography. Heart 2003;89:342–8.

[23] Tang MX, Mulvana H, Gauthier T, Lim AK, Cosgrove DO, Eckersley RJ, et al. Quantitative contrast-enhanced ultrasound imaging: a review of sources of variability. Interface Focus 2011;1:520–39.

[24] Wu J, Tong J. Measurements of the nonlinearity parameter B/A of contrast agents. Ultrasound Med Biol 1998;24:153–9.

[25] Browning RJ, Mulvana H, Tang MX, Hajnal JV, Wells DJ, Eckersley RJ. Effect of albumin and dextrose concentration on ultrasound and microbubble mediated gene transfection in vivo. Ultrasound Med Biol 2012;38:1067–77.

[26] Hernot S, Klibanov AL. Microbubbles in ultrasound-triggered drug and gene delivery. Adv Drug Deliv Rev 2008;60:1153–66.

[27] Rooze J, Rebrov EV, Schouten JC, Keurentjes JT. Dissolved gas and ultrasonic cavitation—a review. Ultrason Sonochem 2013;20:1–11.

[28] Johansen P. Mechanical heart valve cavitation. Expert Rev Med Devices 2004; 1:95–104.

[29] Johansen P, Travis BR, Paulsen PK, Nygaard H, Hasenkam JM. Cavitation caused by mechanical heart valve prostheses — a review. APMIS 2003;111:108–12.

[30] Bessereau J, Genotelle N, Chabbaut C, Huon A, Tabah A, Aboab J, et al. Long-term outcome of iatrogenic gas embolism. Intensive Care Med 2010;36:1180–7.

[31] Engelman R. The neurologic complications of cardiac surgery: introduction. Semin Thorac Cardiovasc Surg 2001;13:147–8.

[32] Baker RA, Andrew MJ, Knight JL. Evaluation of neurologic assessment and outcomes in cardiac surgical patients. Semin Thorac Cardiovasc Surg 2001;13:149–57.

[33] Hammon JW, Stump DA, Butterworth JB, Moody DM. Approaches to reduce neurologic complications during cardiac surgery. Semin Thorac Cardiovasc Surg 2001;13:184–91.

[34] Gorelick PB. Stroke prevention therapy beyond antithrombotics: unifying mechanisms in ischemic stroke pathogenesis and implications for therapy: an invited review. Stroke 2002;33:862–75.

[35] Brott T, Bogousslavsky J. Drug therapy — treatment of acute ischemic stroke. N Engl J Med 2000;343:710–22.

[36] Butler BD, Hills BA. The lung as a filter for microbubbles. J Appl Physiol Respir Environ Exerc Physiol 1979;47:537–43.

[37] Germonpre P, Dendale P, Unger P, Balestra C. Patent foramen ovale and decompression sickness in sports divers. J Appl Physiol 1998;84:1622–6.

[38] Balestra C, Marroni A, Farkas B, Peetrons P, Vanderschueren F, Duboc E, et al. The fractal approach as a tool to understand asymptomatic brain hyperintense MRI signals. Fractals 2004;12:67–72.

[39] Madden D, Lozo M, Dujic Z, Ljubkovic M. Exercise after SCUBA diving increases the incidence of arterial gas embolism. J Appl Physiol 2013;115:716–22.

[40] Tortora GJ, Derrickson BH. Principles of anatomy & physiology. Chapter The cardiovascular system: blood vessels and hemodynamics. 13th ed. John Wiley & Sons, Inc.; 2012. p. 816.

[41] Spencer MP, Oyama Y. Pulmonary capacity for dissipation of venous gas emboli. Aerosp Med 1971;42:822–7.

[42] Francis TJR, Mitchell SJ. Chap.10.4 Pathophysiology of decompression sickness. In: Brubakk AO, Neuman TS, editors. Bennett and Elliott's physiology and medicine of diving. Saunders; 2003. p. 530–56.

[43] Harvey CJ, Blomley MJ, Eckersley RJ, Heckemann RA, Butler-Barnes J, Cosgrove DO. Pulse-inversion mode imaging of liver specific microbubbles: improved detection of subcentimetre metastases. Lancet 2000;355:807–8.

[44] Kostoglou M, Karapantsios TD. Bubble dynamics during the non-isothermal degassing of liquids. Exploiting microgravity conditions. Adv Colloid Interface Sci 2007;134–35:125–37.

[45] Jones SF, Evans GM, Galvin KP. Bubble nucleation from gas cavities — a review. Adv Colloid Interface Sci 1999;80:27–50.

[46] Karapantsios TD, Kostoglou M, Divinis N, Bontozoglou V. Nucleation, growth and detachment of neighboring bubbles over miniature heaters. Chem Eng Sci 2008;63:3438–48.

[47] Divinis N, Karapantsios TD, Kostoglou M, Panoutsos CS, Bontozoglou V, Michels AC, et al. Bubbles growing in supersaturated solutions at reduced gravity. AIChE J 2004;50:2369–82.

[48] Divinis N, Kostoglou M, Karapantsios TD, Bontozoglou V. Self-similar growth of a gas bubble induced by localized heating: the effect of temperature-dependent transport properties. Chem Eng Sci 2005;60:1673–83.

[49] Divinis N, Karapantsios TD, de Bruijn R, Kostoglou M, Bontozoglou V, Legros JC. Bubble dynamics during degassing of liquids at microgravity conditions. AIChE J 2006;52:3029–40.

[50] Mikic BB, Rohsenow WM, Griffith P. On bubble growth rates. Int J Heat Mass Transf 1970;13:657–66.

[51] Plesset MS, Zwick SA. The growth of vapor bubbles in superheated liquids. J Appl Phys 1954;25:493–500.

[52] Scriven LE. On the dynamics of phase growth: L. E. Scriven, Chem. Engng. Sci. 10: 1–13, 1959. Chem Eng Sci 1995;50:3905.

[53] Rayleigh L. Pressure due to collapse of bubbles. Philos Mag 1917:94.

[54] Thuy LT, Weiland RH. Mechanisms of gas desorption from aqueous solution. Ind Eng Chem Fundam 1976;15:286–93.

[55] Weiland RH, Thuy LT, Liveris AN. Transition from bubbling to quiescent desorption of dissolved-gases. Ind Eng Chem Fundam 1977;16:332–5.

[56] Lubetkin SD. Why is it much easier to nucleate gas bubbles than theory predicts? Langmuir 2003;19:2575–87.

[57] Schweitzer PH, Szebehely VG. Gas evolution in liquids and cavitation. J Appl Phys 1950;21:1218–24.

[58] Burrows G, Preece F. The process gas evolution from low vapor pressure liquids upon reduction of pressure. Trans Inst Chem Eng 1954;32:84–9.

[59] Langlois WE. Similarity rules for isothermal bubble growth. J Fluid Mech 1963;15:111–8.

[60] Epstein PS, Plesset MS. On the stability of gas bubbles in liquid–gas solutions. J Chem Phys 1950;18:1505–9.

[61] Bara M, Katz Y. Microbubbles: pathophysiology and clinical implications. Chest 2005;128:2918–32.

[62] Duncan PB, Needham D. Test of the Epstein–Plesset model for gas microparticle dissolution in aqueous media: effect of surface tension and gas undersaturation in solution. Langmuir 2004;20:2567–78.

[63] Kierzkowska-Pawlak H, Chacuk A. Pressure swing absorption of carbon dioxide in DMEPEG solutions. Environ Prot Eng 2009;35:37–45.

[64] Hikita H, Konishi Y. Desorption of carbon-dioxide from supersaturated water in an agitated vessel. AIChE J 1984;30:945–51.

[65] Chappell MA, Payne SJ. The effect of cavity geometry on the nucleation of bubbles from cavities. J Acoust Soc Am 2007;121:853–62.

[66] Chappell MA, Payne SJ. A physiological model of the release of gas bubbles from crevices under decompression. Respir Physiol Neurobiol 2006;153:166–80.

[67] Burrows CF, Bovee KC. Metabolic changes due to experimentally induced rupture of the canine urinary bladder. Am J Vet Res 1974;35:1083–8.

[68] Colin C, Fabre J, McQuillen J. Bubble and slug flow at microgravity conditions: State of knowledge and open questions. Chem Eng Commun 1996;141:155–73.

[69] Duhar G, Colin C. Dynamics of bubble growth and detachment in a viscous shear flow. Phys Fluids 2006;18.

[70] Duhar G, Colin C. A predictive model for the detachment of bubbles injected in a viscous shear flow with small inertial effects. Phys Fluids 2004;16:L31–4.

[71] Klausner JF, Mei R, Bernhard DM, Zeng LZ. Vapor bubble departure in forced-convection boiling. Int J Heat Mass Transf 1993;36:651–62.

[72] Arieli R, Marmur A. Evolution of bubbles from gas micronuclei formed on the luminal aspect of ovine large blood vessels. Respir Physiol Neurobiol 2013;188:49–55.

[73] Papadopoulou V, Evgenidis S, Eckersley RJ, Balestra C, Tang M-X, Karapantsios T. Decompression induced bubble growth on tissue surfaces from gas saturated solutions. In: Bennett M, Davis M, Brandt Corstius J, Germonpré P, editors. Tri-continental scientific meeting on diving and hyperbaric medicine (22–28 Sep 2013); 2013. p. P-27 [Reunion Island].

[74] Chappell MA, Uzel S, Payne SJ. Modeling the detachment and transport of bubbles from nucleation sites in small vessels. Biomed Eng IEEE Trans 2007;54:2106–8.

[75] Lango T, Morland T, Brubakk AO. Diffusion coefficients and solubility coefficients for gases in biological fluids and tissues: a review. Undersea Hyperb Med 1996;23:247–72.

[76] Kabalnov A, Klein D, Pelura T, Schutt E, Weers J. Dissolution of multicomponent microbubbles in the bloodstream: 1. Theory. Ultrasound Med Biol 1998; 24:739–49.

[77] Srinivasan RS, Gerth WA, Powell MR. A mathematical model of diffusion-limited gas bubble dynamics in tissue with varying diffusion region thickness. Respir Physiol 2000;123:153–64.

[78] Srinivasan RS, Gerth WA, Powell MR. Mathematical models of diffusion-limited gas bubble dynamics in tissue. J Appl Physiol 1999;86:732–41.

[79] Van Liew HD, Conkin J, Burkard ME. The oxygen window and decompression bubbles: estimates and significance. Aviat Space Environ Med 1993;64:859–65.

[80] Van Liew HD, Burkard ME. Bubbles in circulating blood: stabilization and simulations of cyclic changes of size and content. J Appl Physiol 1995;79:1379–85.

[81] Hlastala MP, Van Liew HD. Absorption of in vivo inert gas bubbles. Respir Physiol 1975;24:147–58.

[82] Dexter F, Hindman BJ. Recommendations for hyperbaric oxygen therapy of cerebral air embolism based on a mathematical model of bubble absorption. Anesth Analg 1997;84:1203–7.

[83] Branger AB, Eckmann DM. Theoretical and experimental intravascular gas embolism absorption dynamics. J Appl Physiol 1999;87:1287–95.

[84] Eckmann DM, Branger AB, Cavanagh DP. Gas embolism. N Engl J Med 2000; 342:2000–1 [author reply 1–2].

[85] Branger AB, Lambertsen CJ, Eckmann DM. Cerebral gas embolism absorption during hyperbaric therapy: theory. J Appl Physiol 2001;90:593–600.

[86] Branger AB, Eckmann DM. Accelerated arteriolar gas embolism reabsorption by an exogenous surfactant. Anesthesiology 2002;96:971–9.

[87] Eckmann DM, Armstead SC. Surfactant reduction of cerebral infarct size and behavioral deficit in a rat model of cerebrovascular arterial gas embolism. J Appl Physiol 2013 Sep;115(6):868–76.

[88] Rayleigh L. VIII. On the pressure developed in a liquid during the collapse of a spherical cavity. Philos Mag Ser 6 1917;34:94–8.

[89] Plesset MS. The dynamics of cavitation bubbles. ASME J Appl Mech 1949;16:228.

[90] Leighton TG. The acoustic bubble. London: Academic Press; 1994.

[91] Khismatullin DB. Gas microbubbles and their use in medicine. In: Doinikov AA, editor. Bubble and Particle Dynamics in Acoustic Fields: Modern Trends and Applications. Kerala Research Signpost; 2005. p. 231–89.

[92] Khismatullin DB, Nadim A. Radial oscillations of encapsulated microbubbles in viscoelastic liquids. Phys Fluids 2002;14:3534–57.

[93] Prosperetti A. The thermal-behavior of oscillating gas-bubbles. J Fluid Mech 1991;222:587–616.

[94] Frinking PJA, de Jong N. Acoustic modeling of shell-encapsulated gas bubbles. Ultrasound Med Biol 1998;24:523–33.

[95] Bouakaz A, Frinking PJ, de Jong N, Bom N. Noninvasive measurement of the hydrostatic pressure in a fluid-filled cavity based on the disappearance time of micrometer-sized free gas bubbles. Ultrasound Med Biol 1999;25:1407–15.

[96] Sboros V, MacDonald CA, Pye SD, Moran CM, Gomatam J, McDicken WN. The dependence of ultrasound contrast agents backscatter on acoustic pressure: theory versus experiment. Ultrasonics 2002;40:579–83.

[97] Church CC. The effects of an elastic solid-surface layer on the radial pulsations of gas-bubbles. J Acoust Soc Am 1995;97:1510–21.

[98] Vos HJ, Dollet B, Bosch JG, Versluis M, de Jong N. Nonspherical vibrations of microbubbles in contact with a wall—a pilot study at low mechanical index. Ultrasound Med Biol 2008;34:685–8.

[99] Crum LA. Measurements of the growth of air bubbles by rectified diffusion. J Acoust Soc Am 1980;68:203–11.

[100] Nichols W, O'Rourke M, Vlachopoulos C. McDonald's blood flow in arteries. 6 ed. CRC Press; 2001.

[101] Moss WC. Understanding the periodic driving pressure in the Rayleigh–Plesset equation. J Acoust Soc Am 1997;101:1187–90.

[102] Allen JS, Roy RA. Dynamics of gas bubbles in viscoelastic fluids. II. Nonlinear viscoelasticity. J Acoust Soc Am 2000;108:1640–50.

[103] Fung YC. Biomechanics: circulation. 2nd edition. New York: Springer; 1997.

[104] Bull JL. Cardiovascular bubble dynamics. Crit Rev Biomed Eng 2005;33:299–346.

[105] Pozrikidis C. Numerical simulation of the flow-induced deformation of red blood cells. Ann Biomed Eng 2003;31:1194–205.

[106] Halpern D, Secomb TW. The squeezing of red-blood-cells through parallel-sided channels with near-minimal widths. J Fluid Mech 1992;244:307–22.

[107] Secomb TW, Hsu R, Pries AR. Blood flow and red blood cell deformation in nonuniform capillaries: effects of the endothelial surface layer. Microcirculation 2002;9:189–96.

[108] He XJ, Ku DN. Pulsatile flow in the human left coronary artery bifurcation: average conditions. J Biomech Eng 1996;118:74–82.

[109] Ku DN. Blood flow in arteries. Annu Rev Fluid Mech 1997;29:399–434.

[110] Edwards DA, Brenner H, Wasan DT. Interfacial transport processes and rheology. Boston, MA: Butterworth-Heinemann; 1991.

[111] Evgenidis SP, Kazakis NA, Karapantsios TD. Bubbly flow characteristics during decompression sickness: effect of surfactant and electrolyte on bubble size distribution. Colloid Surf A 2010;365:46–51.

[112] Eckmann DM, Diamond SL. Surfactants attenuate gas embolism-induced thrombin production. Anesthesiology 2004;100:77–84.

[113] Hanwright J, Zhou J, Evans GM, Galvin KP. Influence of surfactant on gas bubble stability. Langmuir 2005;21:4912–20.

[114] Ackles K, editor. Symposium on blood–bubble interaction in decompression sickness. Canada: Defence R&D Canada (DRDC), previously DCIEM; December 1973.

[115] Ward CA, McCullough D, Fraser WD. Relation between complement activation and susceptibility to decompression sickness. J Appl Physiol 1987;62:1160–6.

[116] Baz A, Abdel-Khalik SI. Effect of intravascular bubbles on perfusate flow and gas elimination rates following simulated decompression of a model tissue. Undersea Biomed Res 1986;13:27–44.

[117] Lindner JR, Coggins MP, Kaul S, Klibanov AL, Brandenburger GH, Ley K. Microbubble persistence in the microcirculation during ischemia/reperfusion and inflammation is caused by integrin- and complement-mediated adherence to activated leukocytes. Circulation 2000;101:668–75.

[118] Suzuki A, Armstead SC, Eckmann DM. Surfactant reduction in embolism bubble adhesion and endothelial damage. Anesthesiology 2004;101:97–103.

[119] Zakin JL, Bewersdorff HW. Surfactant drag reduction. Rev Chem Eng 1998;14:253–320.

[120] Sawchuk AP, Unthank JL, Dalsing MC. Drag reducing polymers may decrease atherosclerosis by increasing shear in areas normally exposed to low shear stress. J Vasc Surg 1999;30:761–4.

[121] Kobayashi S, Crooks SD, Eckmann DM. In vitro surfactant mitigation of gas bubble contact-induced endothelial cell death. Undersea Hyperb Med 2011;38:27–39.

[122] Miller R, Policova Z, Sedev R, Neumann AW. Relaxation behaviour of human albumin adsorbed at the solution/air interface. Colloids Surf A Physicochem Eng Asp 1993;76:179–85.

[123] Hunter JR, Kilpatrick PK, Carbonell RG. β-Casein adsorption at the air/water interface. J Colloid Interface Sci 1991;142:429–47.

[124] Stride E. The influence of surface adsorption on microbubble dynamics. Philos Transact A Math Phys Eng Sci 2008;366:2103–15.

[125] Lindner JR, Ismail S, Spotnitz WD, Skyba DM, Jayaweera AR, Kaul S. Albumin microbubble persistence during myocardial contrast echocardiography is associated with microvascular endothelial glycocalyx damage. Circulation 1998;98:2187–94.

[126] Eckmann DM, Cavanagh DP, Branger AB. Wetting characteristics of aqueous surfactant-laden drops. J Colloid Interface Sci 2001;242:386–94.

[127] Thorsen T, Dalen H, Bjerkvig R, Holmsen H. Transmission and scanning electron microscopy of N2 microbubble-activated human platelets in vitro. Undersea Biomed Res 1987;14:45–58.

[128] Marabotti C, Chiesa F, Scalzini A, Antonelli F, Lari R, Franchini C, et al. Cardiac and humoral changes induced by recreational scuba diving. Undersea Hyperb Med 1999;26:151–8.

[129] Boussuges A, Blanc P, Molenat F, Bergmann E, Sainty JM. Haemoconcentration in neurological decompression illness. Int J Sports Med 1996;17:351–5.

[130] Bove AA, Hallenbeck JM, Elliott DH. Changes in blood and plasma volumes in dogs during decompression sickness. Aerosp Med 1974;45:49–55.

[131] Yanagisawa K, Moriyasu F, Miyahara T, Yuki M, Iijima H. Phagocytosis of ultrasound contrast agent microbubbles by Kupffer cells. Ultrasound Med Biol 2007;33:318–25.

[132] Milo S, Rambod E, Gutfinger C, Gharib M. Mitral mechanical heart valves: in vitro studies of their closure, vortex and microbubble formation with possible medical implications. Eur J Cardiothorac 2003;24:364–70.